

Table 2  
Measurement errors of this system by plotting bone land marks

Trial	Subject 1		Subject 2		Subject 3		Subject 4		Subject 5	
	FTA	HKA	FTA	HKA	FTA	HKA	FTA	HKA	FTA	HKA
1	178.9	-5.0	179.7	-6.7	184.2	-10.2	185.6	-10.4	184.1	-7.1
2	179.0	-5.1	179.9	-6.8	184.0	-10.4	185.5	-10.5	184.0	-7.1
3	178.9	-5.0	179.9	-6.7	184.0	-10.2	185.5	-10.4	184.2	-6.9
4	178.9	-5.1	179.7	-6.6	184.1	-10.4	185.4	-10.6	184.3	-7.1
5	178.9	-4.9	179.7	-6.7	184.0	-10.4	185.7	-10.5	184.1	-7.2
Error range	0.1	0.2	0.2	0.2	0.3	0.3	0.3	0.3	0.3	0.2

with five subjects. The error range was within  $0.3^\circ$  for both HKA and FTA (Table 2). This appears to be acceptable for assessment of lower limb alignment.

A limitation of this study was comparability of CT scans taken in a supine position to radiographs taken in a weight-bearing position. Generally, lower limb alignment is measured using AP long-standing radiographs. Although we did not obtain CT images in the standing position, we used CT images in a semi-standing position, taken with the knee in full extension and the ankle joint at  $90^\circ$  of flexion with an ankle brace in the supine position.

#### Acknowledgements

This work was partly supported by the Research for the Future Program of the Japan Society for the Promotion of Science (JSPS), JSPS-RFTF99I00901.

#### References

- [1] Bauer GC, Insall J, Koshino T. Tibial osteotomy in gonarthrosis. *J Bone Joint Surg Am* 1969;51(8):1545–63.
- [2] Berger RA, Rubash HE, Seel MJ, et al. Determining the rotational alignment of the femoral component in total knee arthroplasty using the epicondylar axis. *Clin Orthop* 1993; 286(January):40–7.
- [3] Berman AT, Bosacco SJ, Kirshner S, et al. Factors influencing long-term results in high tibial osteotomy. *Clin Orthop* 1991; 272(November):192–8.
- [4] Chao EY, Sim FH. Computer-aided preoperative planning in knee osteotomy. *Iowa Orthop J* 1995;15:4–18.
- [5] Coventry MB, Ilstrup DM, Wallrichs SL. Proximal tibial osteotomy. A critical long-term study of eighty-seven cases. *J Bone Joint Surg Am* 1993;75(2):196–201.
- [6] Ellis RE, Tso CY, Rudan JF, Harrison MM. A surgical planning and guidance system for high tibial osteotomy. *Comput Aided Surg* 1999;4(5):264–74.
- [7] Hernigou P, Medevielle D, Debeyre J, Goutallier D. Proximal tibial osteotomy for osteoarthritis with varus deformity. A ten to thirteen-year follow-up study. *J Bone Joint Surg Am* 1987;69(3): 332–54.
- [8] Insall JN, Dorr LD, Scott RD, et al. Rationale of the Knee Society clinical rating system. *Clin Orthop* 1989;248(November):13–4.
- [9] Insall JN, Joseph DM, Msika C. High tibial osteotomy for varus gonarthrosis. A long-term follow-up study. *J Bone Joint Surg Am* 1984;66(7):1040–8.
- [10] Ivarsson I, Myrnerström R, Gillquist J. High tibial osteotomy for medial osteoarthritis of the knee. A 5 to 7 and 11 year follow-up. *J Bone Joint Surg Br* 1990;72(2):238–44.
- [11] Kellgren JH, Lawrence JS. Radiological assessment of osteoarthritis. *Ann Rheum Dis* 1957;6:494–502.
- [12] Kettelkamp DB, Wenger DR, Chao EY, Thompson C. Results of proximal tibial osteotomy. *J Bone Joint Surg Am* 1976;58(7):952–60.
- [13] Krackow KA, Matthew JP. High tibial osteotomy and distal femoral osteotomy for valgus or varus deformity around the knee. *AAOS Instructional Course Lecture*, vol. 47, 1998. p. 429–36.
- [14] Krackow KA, Pepe CL, Galloway EJ. A mathematical analysis of the effect of flexion and rotation on apparent varus/valgus alignment at the knee. *Orthopedics* 1990;13(8):861–8.
- [15] MacIntosh DL, Welsh RP. Joint debridement—a complement to high tibial osteotomy in the treatment of degenerative arthritis of the knee. *J Bone Joint Surg Am* 1977;59(8):1094–7.
- [16] Moreland JR, Bassett LW, Hanker GJ. Radiographic analysis of the axial alignment of the lower extremity. *J Bone Joint Surg Am* 1987;69(5):745–9.
- [17] Rinonapoli E, Mancini GB, Corvaglia A, Musciello S. Tibial osteotomy for varus gonarthrosis. A 10- to 21-year followup study. *Clin Orthop* 1998;353(Aug):185–93.
- [18] Ritter MA, Fechtman RA. Proximal tibial osteotomy. A survivorship analysis. *J Arthroplasty* 1988;3(4):309–11.
- [19] Rudan JF, Simurda MA. Valgus high tibial osteotomy. A long-term follow-up study. *Clin Orthop* 1991;268(July):157–60.
- [20] Swanson KE, Stocks GW, Warren PD, et al. Does axial limb rotation affect the alignment measurements in deformed limbs? *Clin Orthop* 2000;371(February):246–52.
- [21] Vainionpää S, Laike E, Kirves P, Tiisanen P. Tibial osteotomy for osteoarthritis of the knee. A five to ten-year follow-up study. *J Bone Joint Surg Am* 1981;63(6):938–46.
- [22] Wright JG, Treble N, Feinstein AR. Measurement of lower limb alignment using long radiographs. *J Bone Joint Surg Br* 1991; 73(5):721–3.
- [23] Yasuda K, Majima T, Tsuchida T, Kaneda K. A ten- to 15-year follow-up observation of high tibial osteotomy in medial compartment osteoarthritis. *Clin Orthop* 1992;282(September):186–95.

# LOW-INTENSITY PULSED ULTRASOUND ACCELERATES MATURATION OF CALLUS IN PATIENTS TREATED WITH OPENING-WEDGE HIGH TIBIAL OSTEOTOMY BY HEMICALLOTASIS

BY NORIYUKI TSUMAKI, MD, MASAOKI KAKIUCHI, MD, JIRO SASAKI, TAKAHIRO OCHI, MD, AND HIDEKI YOSHIKAWA, MD

*Investigation performed at the Department of Orthopaedics, Osaka University Graduate School of Medicine,  
and the Department of Orthopaedic Surgery and Radiology, Osaka Police Hospital, Osaka, Japan*

**Background:** Opening-wedge high tibial osteotomy by hemicallotasis for osteoarthritis in the medial compartment of the knee requires external fixation for a long time, until callus maturation is complete. The aim of this study was to determine if low-intensity pulsed ultrasound would accelerate callus maturation when applied after distraction to limbs treated with opening-wedge high tibial osteotomy by hemicallotasis.

**Methods:** Twenty-one patients with symmetric grades of osteoarthritis and similar degrees of varus deformity in the two knees underwent bilateral one-stage opening-wedge high tibial osteotomy by hemicallotasis. After completion of distraction, the bone mineral density of the distraction callus was measured. Then, one randomly selected limb was subjected to ultrasound treatment for twenty minutes daily until removal of the external fixator. The contralateral limb was left untreated to serve as the control. After four weeks of treatment, bone mineral density was measured again.

**Results:** During the four-week treatment period, the mean increase in callus bone mineral density was significantly greater in the ultrasound-treated tibiae ( $0.20 \pm 0.12 \text{ g/cm}^2$ ) than in the control tibiae ( $0.13 \pm 0.10 \text{ g/cm}^2$ ) ( $p = 0.02$ , unpaired t test). In eighteen patients the increase in the bone mineral density was greater in the ultrasound-treated limb than in the control limb, whereas in three patients the increase was greater in the control limb.


**Conclusions:** We found that low-intensity pulsed ultrasound applied during the consolidation phase of distraction osteogenesis accelerates callus maturation after opening-wedge high tibial osteotomy by hemicallotasis in elderly patients.

**Level of Evidence:** Therapeutic study, Level I-1a (randomized controlled trial [significant difference]). See Instructions to Authors for a complete description of levels of evidence.

Ultrasound, a form of mechanical energy that produces micromechanical strain when transmitted through the body, is widely used in medicine as a therapeutic and diagnostic tool. *In vitro* studies have demonstrated that low-intensity pulsed ultrasound alters metabolism at the cellular level. Micromechanical strain caused by ultrasound transmission through the body can promote bone formation in a manner comparable with the bone responses to mechanical stress postulated by Wolff's law<sup>1,2</sup>. Studies of animals have

demonstrated that low-intensity pulsed ultrasound increases the rate of endochondral bone formation and the structural strength of fracture sites<sup>3,4</sup>. Clinical investigations have shown that low-intensity pulsed ultrasound improves healing of pseudoarthroses, delayed unions, and nonunions<sup>5,6</sup>. Randomized, double-blind, controlled clinical trials have shown that the technique accelerates the repair process in fractures of the tibia<sup>7</sup> and radius<sup>8</sup>. These studies have established the clinical usefulness of low-intensity pulsed ultrasound for acceleration of fracture-healing<sup>9</sup>.

Callotasis and hemicallotasis are useful techniques to correct limb deformity or to lengthen the limb<sup>9</sup>, but the distraction callus heals very slowly, requiring patients to wear an

 A commentary is available with the electronic versions of this article, on our web site ([www.jbjs.org](http://www.jbjs.org)) and on our quarterly CD-ROM (call our subscription department, at 781-449-9780, to order the CD-ROM).

external fixator for a long period. The effects of low-intensity pulsed ultrasound on healing of the distraction callus have been examined in animal models<sup>19,20</sup> but have not been assessed in a clinical setting, to our knowledge.

Opening-wedge high tibial osteotomy by hemicallotasis, a surgical intervention for patients with osteoarthritis in the medial compartment of the knee, has the advantage of accurate correction<sup>15</sup>. However, the technique requires external fixation until the distraction callus is mature, and a high rate of pin-site infection has been reported<sup>16</sup>.

In this randomized study, we quantitatively examined the effects of low-intensity pulsed ultrasound on the maturation of the distraction callus during the consolidation phase in patients treated with an opening-wedge high tibial osteotomy by hemicallotasis.

## Materials and Methods

### Patient Selection

From 1999 to 2002, bilateral one-stage opening-wedge high tibial osteotomy by hemicallotasis was performed in thirty-three patients who had bilateral osteoarthritis in the medial compartment of the knee with bilateral knee pain. Selection criteria for the present study included (1) bilaterally symmetric grades of osteoarthritis according to the classification of Kellgren and Lawrence<sup>21</sup>, and (2) a difference of  $\leq 3^\circ$  in varus deformity between the left and right sides as indicated by the femorotibial angles measured on full-length radiographs of the lower limbs with the patient standing. Twenty-one patients (seventeen women and four men) who met these criteria consented to participate in the study. The ages of the patients ranged from fifty-three to seventy-eight years (average, sixty-eight years). The severity of the medial osteoarthritis was grade 2 in four knees, grade 3 in thirty knees, and grade 4 in eight knees. The study was approved by our hospital review board.

### Operative Technique

Opening-wedge high tibial osteotomy was performed with use of an articulated dynamic axial fixator with a proximal T-clamp (hemicallotasis device; Orthofix 20-010 and CP-0029; Orthofix, Bussolengo, Italy). During the surgery, four tapered half-pins (Orthofix; 6 mm/5 mm) were inserted; two with cancellous threads were placed at the proximal sites and two with cortical threads, at the distal sites. For the osteotomy, an anteromedial approach was used, with a transverse incision of the skin and a longitudinal incision of the periosteum followed by elevation. The position and direction of the osteotomy were monitored in both the coronal and the sagittal plane with use of radiography during the operation. Osteotomy of the medial three-quarters of the proximal part of the tibia was carried out just proximal to the tibial tubercle. We used an osteotome to cut the anterior and middle portions of the tibia, and we used an oscillating saw to cut the posterior cortex. The status of the cortex lateral to the osteotomy site was assessed by testing the rigidity of the osteotomy site with manual valgus stress. The Orthofix fixator was applied, and distraction

was performed for 5 mm to ensure that the intact portion lateral to the osteotomy site acted as a hinge. Then the fixator was compressed so that there was good osseous apposition. The periosteum was closed. A fibular osteotomy was not performed. As with callus distraction for limb-lengthening, the osteotomy was followed by periods of latency, distraction, and consolidation until removal of the external fixator. Patients were allowed full weight-bearing throughout these periods.

### Distraction and Consolidation

After a latency period of fourteen days, distraction was begun. Radiographs of the osteotomy sites in both limbs were made once a week throughout the distraction and consolidation phases. Additional radiographs were made according to the symptoms and findings of previous radiographs. The compression/distraction unit was elongated at a rate of 1 mm daily, with two 0.5-mm distractions each day. Distraction was stopped and the consolidation phase was begun when the hip-ankle mechanical axis of the limb passed the medial one-ninth to one-third of the lateral compartment of the tibial plateau as seen on a full-length radiograph of the limb with the patient standing. The locking bolt of the telescopic body of the fixator was then tightened.

The consolidation period was ended when the callus was considered strong enough for safe removal of the fixator without the risk of fracture (i.e., when there was a smooth uninterrupted cortical margin medial to the regenerated bone or an uninterrupted trabecular pattern occupying the lateral two-thirds of the tibia on an anteroposterior radiograph). The assessors of callus consolidation were not blinded to the use of low-intensity pulsed ultrasound. A few days after release of the locking screw (at a mean [and standard deviation] of  $1.5 \pm 0.6$  days; range, one to three days), the fixator was removed and the pins were left in place for a trial period of several more days. The pins were removed after radiographs confirmed that there was no evidence of collapse of the callus.

### Measurement of Bone Mineral Density

Although we performed the osteotomy perpendicular to the long axis of the lower limb in the sagittal plane, the postoperative anteroposterior radiograph of the proximal part of the tibia revealed that the osteotomy was not perfectly parallel to the x-ray beam in some patients. Before measuring bone mineral density, all patients were placed in the supine position with the knees in neutral rotation under the x-ray tube. The knee joint was slightly flexed (Fig. 1-A) or the entire limb was raised (Fig. 1-B), so that the beam would pass parallel to the osteotomy. As a result, we obtained an anteroposterior view of the callus without an overlap of the anterior or posterior cortical bone of the tibia. We carefully recorded the position of each limb of each patient by measuring the distance and angle of the fixators relative to the bed on which the patient lay. To measure the bone mineral density of the distraction callus, the patient was then placed on a dual-energy x-ray absorptiometry unit (QDR-2000; Hologic, Boston, Massachusetts) with the limb in the same position as determined under the x-ray

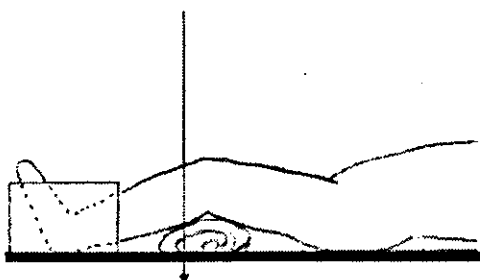


Fig. 1-A

Measurement of bone mineral density. The knee joint was slightly flexed (Fig. 1-A) or the entire limb was raised (Fig. 1-B), so that the beam would pass parallel to the osteotomy. The limb was positioned by referring to the position of the fixators, which were determined on radiographs.

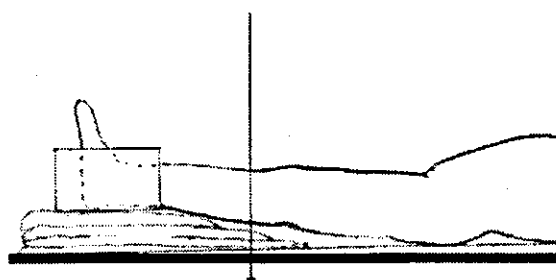


Fig. 1-B

tube. Bone mineral density was expressed in grams per square centimeter. On the view obtained from the scan, we confirmed that the callus was visible without overlap of anterior or posterior cortical bone of the tibia, indicating that the beam was parallel to the osteotomy. Two regions of interest in each tibia were selected for measurement of regional bone mineral density with use of QDR for Windows software (version 11.2; Hologic). Following the previously described method with modification<sup>3</sup>, we selected one region of interest within the distraction gap (Fig. 1-C). The other was in the segment just distal to the distraction gap (Fig. 1-D). The region of interest in the distal segment was 8 mm in height and spanned the medial half of the tibia. The reproducibility error of the results was evaluated with three consecutive measurements and was found to be <3%. To test day-to-day reproducibility, a bone phantom (Hologic) was attached with a metal pin 5 cm above the bed, and its bone mineral density was measured daily for

one month. The coefficient of variation was 0.8%.

The bone mineral density of the callus was measured twice for each tibia: at the start of the consolidation period and four weeks after the start of the consolidation period. The first bone mineral density measurement was subtracted from the second to calculate the increase in bone mineral density over the four-week consolidation period.

#### Application of Ultrasound

For each patient, the limb to be treated with low-intensity pulsed ultrasound was randomly selected with use of a random-number generator on a computer. Ultrasound energy was provided by a Sonic Accelerated Fracture Healing System (SAFHS; Exogen, Piscataway, New Jersey). The treatment head module delivered an ultrasound signal composed of a burst width of 200  $\mu$ sec containing 1.5-MHz sine waves, with a repetition rate of 1 kHz and a spatial average-temporal average

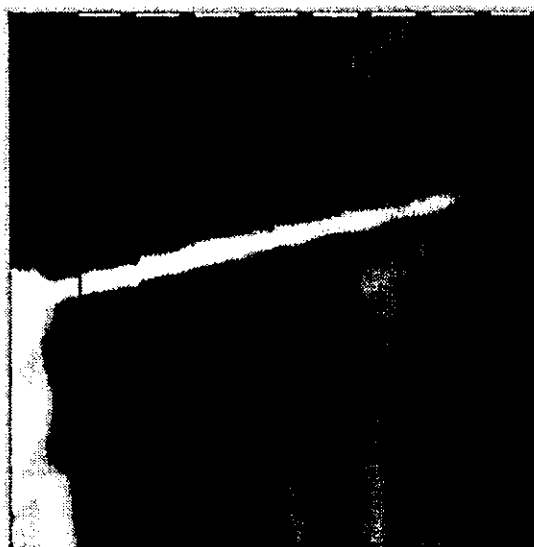


Fig. 1-C



Fig. 1-D

Anteroposterior images produced by a dual-energy x-ray absorptiometry unit (QDR; Hologic) to measure bone mineral density in the proximal part of a tibia that underwent opening-wedge high tibial osteotomy. The regions of interest of measurement were set within the distraction gap (outlined in red) (Fig. 1-C) and the segment distal to the distraction gap (outlined in red) (Fig. 1-D).

intensity of 30 mW/cm<sup>2</sup>. Within two days after the first bone mineral density measurement, we began daily twenty-minute ultrasound treatments on the one side, and we continued the treatment until the fixator was removed. The treatment head module was positioned on the anteromedial aspect of the proximal part of the leg at the level of the osteotomy and was fixed with a strap. All twenty-one patients were hospitalized until removal of the pins and were assisted by the hospital staff in carrying out the low-intensity pulsed ultrasound treatment.

#### Statistical Analysis

The *t* test was used to compare data between treated and untreated limbs. A *p* value of <0.05 was considered to indicate significance.

### Results

#### Baseline Characteristics

None of the patients had previously undergone knee surgery such as meniscectomy or cruciate ligament repair. The mean weight of the patients was 61 ± 11 kg, and the mean body mass index was 26 ± 3. Three patients smoked during the treatment period.

Preoperatively, the femorotibial angle averaged 185° ± 5° in the ultrasound-treated limbs and 184° ± 5° in the controls, the range of knee flexion measured with manual goniometry averaged 121° ± 27° in the ultrasound-treated limbs and 125° ± 10° in the controls, and the range of knee extension averaged -4° ± 6° in the ultrasound-treated limbs and -3° ± 5° in the controls. Thus, the preoperative varus deformity and ranges of motion did not differ substantially between the ultrasound-treated and control limbs. Preoperatively, four patients had equal pain in the two knees, seven had more knee pain on the side that was later treated with low-intensity pulsed ultrasound, and ten patients had less pain on that side. The mean period of distraction did not differ between the ultrasound-treated tibiae (37 ± 7 days) and the control tibiae (37 ± 7 days). The distraction period was the same for both sides in eighteen patients. It was two days shorter on the ultrasound-treated side in one patient, four days shorter on the ultrasound-treated side in another patient, and three days shorter for the control limb in still another patient.

During the distraction period, patients experienced pain in the lower limbs and were occasionally unable to stand. After the start of the consolidation period, the pain decreased, and all patients walked using a pair of crutches. Pin-track infections developed in six limbs in the ultrasound-treated group and five limbs in the control group. These infections responded to local pin-site care and antibiotic treatment. We did not observe signs of infection at any osteotomy site or in any joint in the limbs.

As a result of randomization, the right limb was chosen for low-intensity pulsed ultrasound and the left limb served as the control in eleven patients. In ten patients, the left limb was chosen for low-intensity pulsed ultrasound and the right limb served as the control.

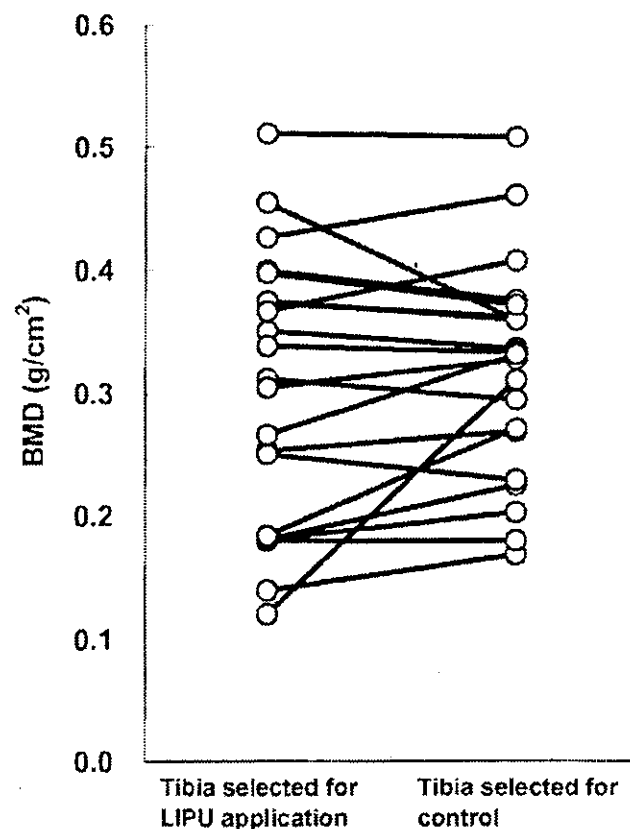
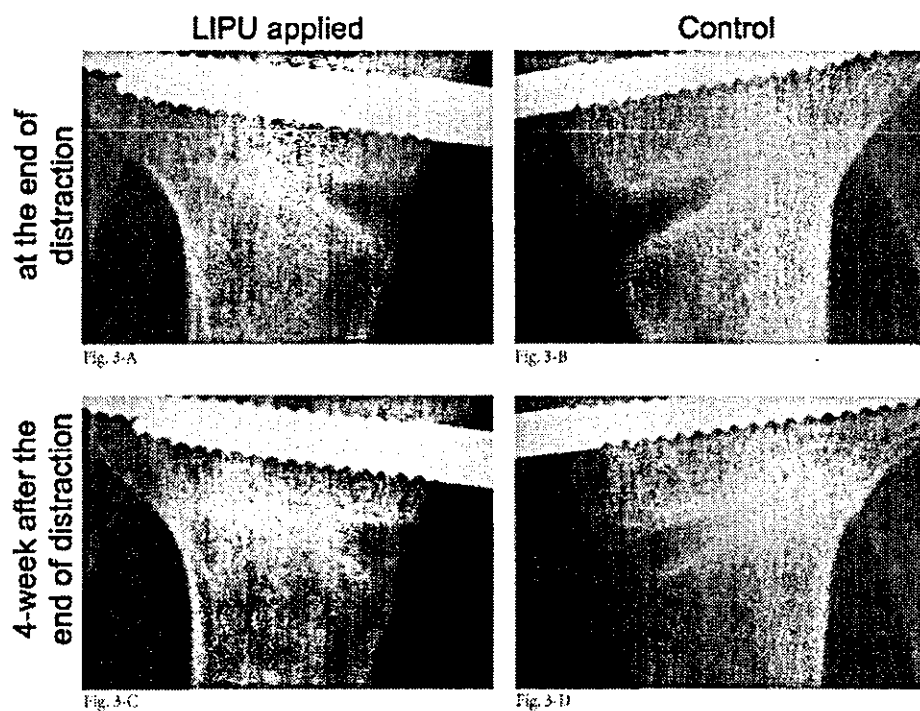


Fig. 2  
Bone mineral density (BMD) of the distraction callus before the start of treatment with low-intensity pulsed ultrasound (LIPU). The tibiae selected for ultrasound treatment are shown on the left, and the control tibiae are shown on the right, with the values for the limbs of the same patient connected by lines. The mean bone mineral density was 0.30 ± 0.11 g/cm<sup>2</sup> in the tibiae selected for ultrasound treatment and 0.32 ± 0.09 g/cm<sup>2</sup> in control tibiae (*p* = 0.31, unpaired *t* test). Note that, in each patient, there was little difference in the callus bone mineral density between the two tibiae, whereas the callus bone mineral density varied more widely among individuals.

#### Bone Mineral Density

Before the start of the treatment with the low-intensity pulsed ultrasound, the bone mineral density of the distraction callus averaged 0.30 ± 0.11 g/cm<sup>2</sup> in the tibiae chosen to be treated with ultrasound and 0.32 ± 0.09 g/cm<sup>2</sup> in the controls (*p* = 0.31, unpaired *t* test) (Fig. 2). The mean increase in bone mineral density during the four-week treatment period was significantly greater in the ultrasound-treated tibiae (0.20 ± 0.12 g/cm<sup>2</sup>) than it was in the controls (0.13 ± 0.10 g/cm<sup>2</sup>) (*p* = 0.02, unpaired *t* test). In eighteen patients, the bone mineral density increased more in the ultrasound-treated limb than in the control limb; in three patients, the bone mineral density increased more in the control limb (Figs. 3-A through 4). Of the three patients who had a greater increase in the control limb, one was a smoker, two had had almost equal pain in the two knees, and one had had more knee pain

**Figs. 3-A through 3-D** Radiographs of a woman who underwent progressive opening-wedge osteotomy by hemicallotasis at the age of sixty-seven years. **Figs. 3-A and 3-B** Radiographs of the proximal parts of the right (Fig. 3-A) and left (Fig. 3-B) tibiae made at the end of distraction show that both limbs contained callus with moderate mineralization. After measurement of bone mineral density, low-intensity pulsed ultrasound (LIPU) was applied only to the right tibia; the left tibia was used as the control. **Figs. 3-C and 3-D** Four weeks later, the callus of the right tibia (Fig. 3-C) appears more consolidated than that of the left tibia (Fig. 3-D). The bone mineral density of the distraction gap was again measured after this four-week consolidation period. The increase in the bone mineral density in the callus was 0.29 g/cm<sup>2</sup> in the right tibia and 0.10 g/cm<sup>2</sup> in the left.



in the ultrasound-treated limb than in the control limb.

The mean increase in bone mineral density in the segment just distal to the distraction gap during the four-week treatment period was  $0.02 \pm 0.09$  g/cm<sup>2</sup> in the ultrasound-treated tibiae and  $-0.03 \pm 0.09$  g/cm<sup>2</sup> in the control tibiae. The difference between the two groups was not significant ( $p = 0.07$ ).

#### Consolidation Period

The mean consolidation period was  $7.1 \pm 2.6$  weeks (range, four to twelve weeks) in the ultrasound-treated group and  $7.9 \pm 2.4$  weeks (range, five to thirteen weeks) in the control group. The consolidation period for the ultrasound-treated limb was shorter than that for the control limb in thirteen patients: it was three weeks shorter for four patients, two weeks shorter for four patients, and one week shorter for five patients. The consolidation period was the same on both sides in six patients, and, in two patients, consolidation occurred one week earlier in the control limb than in the ultrasound-treated limb. The fixators remained in place for a mean of  $14.6 \pm 3.0$  weeks in the ultrasound-treated tibiae and for  $15.5 \pm 2.7$  weeks in the controls.

#### Discussion

Bone-forming activity varies among individuals<sup>11</sup>. This variation may account in part for the difficulties in determining the effects of low-intensity pulsed ultrasound in clinical studies with limited numbers of patients. In the present study, the same surgical procedure was performed on both tibiae of each patient on the same day. Low-intensity pulsed ultrasound was applied on one side, whereas the contralateral side

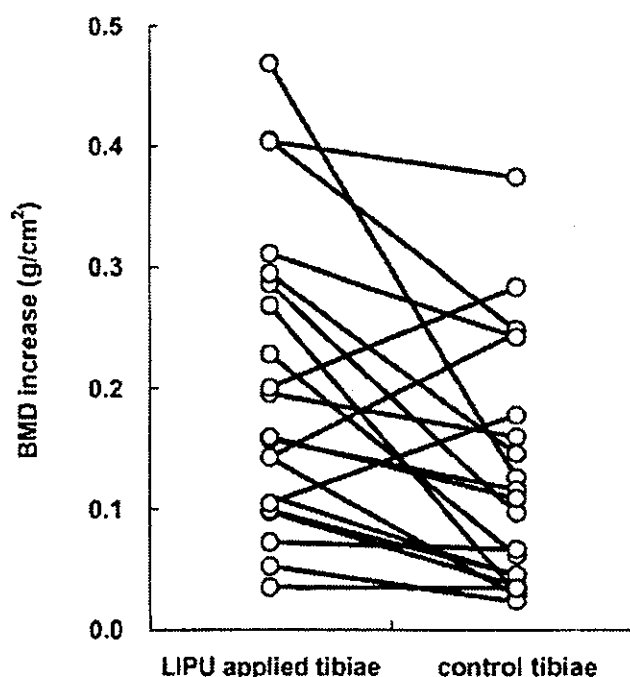


**Fig. 4** Increases in callus bone mineral density (BMD) during the four-week consolidation period in the limbs treated with low-intensity pulsed ultrasound (LIPU) (left) and the control limbs (right), with the values for the limbs of the same patient connected by lines. The mean increase in bone mineral density was  $0.20 \pm 0.12$  g/cm<sup>2</sup> in the ultrasound-treated tibiae and  $0.13 \pm 0.10$  g/cm<sup>2</sup> in the control tibiae ( $p = 0.02$ , unpaired t test).

was used as the internal control. Before the treatment with the low-intensity pulsed ultrasound, the mean difference in callus bone mineral density between the left and right limbs of the same patient was usually relatively small, whereas the callus bone mineral density varied more substantially among individuals (Fig. 2). The increase in bone mineral density during the four-week consolidation period also varied among individuals, suggesting variation in bone-forming activities among patients.

The present study showed that low-intensity pulsed ultrasound significantly enhances the increase in mineralization of the callus during hemicalloplasty, as assessed by measuring bone mineral density. In fact, the external fixators were removed an average of one week earlier from the ultrasound-treated limbs than from the control limbs. In the present study, low-intensity pulsed ultrasound was applied after distraction had ceased, in order to assess the bone mineral density of the distraction callus before the ultrasound treatment. A recent investigation of rabbits showed that low-intensity pulsed ultrasound stimulates bone formation most effectively during the distraction phase<sup>20</sup>. Future clinical studies should address the question of whether additional low-intensity pulsed ultrasound treatment during the distraction phase can further shorten the period necessary for callus maturation.

The effects of low-intensity pulsed ultrasound on maturation of distraction callus have been investigated in several animal studies, with controversial results. In a rabbit study, Shimazaki et al. found that bone mineral density, hard callus area, and mechanical test scores were greater in distraction callus treated with low-intensity pulsed ultrasound than in the control group<sup>21</sup>. In a study of rats, Ebersson et al. found that radiographically assessed healing occurred earlier in ultrasound-treated bones than in control bones and that bone volume fraction and trabecular bone pattern factor were higher in the ultrasound-treated bones<sup>22</sup>. In a study of rabbits, Tis et al. found a greater hard callus area and less fibrous tissue in bones treated with low-intensity pulsed ultrasound than in control bones<sup>23</sup>. Neither Ebersson et al. nor Tis et al. found a difference in bone mineral density or mechanical strength of distraction callus between ultrasound-treated bones and controls, although Ebersson et al. observed a trend toward greater mechanical strength in ultrasound-treated bones. Uglow et al. found no substantial difference in bone mineral content, cross-sectional area, or strength of distraction callus between ultrasound-treated bones and control bones of rabbits<sup>24</sup>. In all of the animal studies mentioned above, osteotomy and distraction were performed at the diaphysis, which consists of thick cortical bone. In the metaphyseal segment adjacent to the distraction callus in the present study, the bone mineral density

tended to increase more in the ultrasound-treated limbs than in the control limbs, although the difference was not significant ( $p = 0.07$ ). Uglow et al. found no significant difference in the reduction of volumetric bone mineral density of the segment adjacent to the distraction callus in the diaphysis between their ultrasound-treated group and control group ( $p > 0.5$ ) in rabbits. Although the applicability of findings of animal studies to human clinical research remains unclear, results obtained from the present study and those of animal studies collectively suggest that metaphyseal trabecular bone might be more susceptible than diaphyseal cortical bone to mechanical forces inherent to low-intensity pulsed ultrasound.

*In vitro* and *in vivo* studies have been performed to investigate the mechanisms by which mechanical stimulation due to low-intensity pulsed ultrasound is translated into a biological response. Low-intensity pulsed ultrasound has effects on chondrocytes<sup>25,26</sup> as well as osteoblasts<sup>27,28</sup>. Rawool et al. reported that low-intensity pulsed ultrasound also stimulates angiogenesis<sup>29</sup>, thus increasing local blood flow. The usefulness of low-intensity pulsed ultrasound in fracture-healing has previously been established<sup>30</sup>. Distraction osteogenesis may involve an ossification process (transchondroid ossification) different from that of fracture-healing<sup>31</sup>. Future studies should include clarification of the distraction osteogenesis-specific mechanism that translates mechanical forces due to low-intensity pulsed ultrasound into bone formation. ■

Noriyuki Tsumaki, MD  
Takahiro Ochi, MD  
Hideki Yoshikawa, MD  
Department of Orthopaedics, Osaka University Graduate School of Medicine, 2-2 Yamadaoka, Suita, Osaka 565-0871, Japan. E-mail address for N. Tsumaki: tsumaki-n@umin.ac.jp

Masaaki Kakuuchi, MD  
Jiro Sasaki  
Departments of Orthopaedic Surgery (M.K.) and Radiology (J.S.), Osaka Police Hospital, 10-31 Kitayama-cho, Tennoji-ku, Osaka 543-0035, Japan

In support of their research or preparation of this manuscript, one or more of the authors received Scientific Research Grant 15390456 from the Ministry of Education, Science and Culture of Japan; Health and Labor Sciences Research Grants of Japan; and Grant 0126 from the Japan Orthopaedic and Traumatology Foundation, Incorporated. None of the authors received payments or other benefits or a commitment or agreement to provide such benefits from a commercial entity. No commercial entity paid or directed, or agreed to pay or direct, any benefits to any research fund, foundation, educational institution, or other charitable or nonprofit organization with which the authors are affiliated or associated.

## References

1. Wolff J. *The law of bone remodeling*. New York: Springer; 1985.
2. Hulskes R, Ruimerman R, van Lonth GH, Janssen JD. Effects of mechanical forces on maintenance and adaptation of form in trabecular bone. *Nature*. 2000;405:704-6.
3. Yang KH, Park SJ. Stimulation of fracture healing in a canine tibia full-defect model by low-intensity pulsed ultrasound. *Kansei Med J*. 2001;42:503-6.
4. Yang KH, Parvizi J, Wang SJ, Lewallen DG, Kinnick RR, Greenleaf JF, Bolander ME. Exposure to low-intensity ultrasound increases aggrecan gene expression in a rat femur fracture model. *J Orthop Res*. 1996;14:800-9.
5. Rubin C, Bolander M, Ryaby JP, Hadjilargyrou M. The use of low-intensity ultrasound to accelerate the healing of fractures. *J Bone Joint Surg Am*. 2001;83:259-70.

6. Heckman JD, Sarasohn-Kahn J. The economics of treating tibia fractures. The cost of delayed unions. *Bull Hosp Jt Dis.* 1997;56:63-72.
7. Heckman JD, Ryaby JP, McCabe J, Frey JJ, Kilcoyne RF. Acceleration of tibial fracture-healing by non-invasive, low-intensity pulsed ultrasound. *J Bone Joint Surg Am.* 1994;76:26-34.
8. Kristiansen TK, Ryaby JP, McCabe J, Frey JJ, Roe LR. Accelerated healing of distal radial fractures with the use of specific, low-intensity ultrasound. A multicenter, prospective, randomized, double-blind, placebo-controlled study. *J Bone Joint Surg Am.* 1997;79:961-73.
9. Paley D. *Principles of deformity correction.* New York: Springer; 2002.
10. Shimazaki A, Inui K, Azuma Y, Nishimura N, Yamano Y. Low-intensity pulsed ultrasound accelerates bone maturation in distraction osteogenesis in rabbits. *J Bone Joint Surg Br.* 2000;82:1077-82.
11. Tis JE, Meffert CR, Inoue N, McCarthy EF, Machen MS, McHale KA, Chao EY. The effect of low intensity pulsed ultrasound applied to rabbit tibiae during the consolidation phase of distraction osteogenesis. *J Orthop Res.* 2002;20:793-800.
12. Machen MS, Tis JE, Inoue N, Meffert RH, Chao EY, McHale KA. The effect of low intensity pulsed ultrasound on regenerate bone in a less-than-rigid biomechanical environment. *Bioelectromagnetics.* 2002;12:239-47.
13. Ebersson CP, Hogan KA, Moore DC, Ehrlich MG. Effect of low-intensity ultrasound stimulation on consolidation of the regenerate zone in a rat model of distraction osteogenesis. *J Pediatr Orthop.* 2003;23:46-51.
14. Uglow MG, Peat RA, Hile MS, Biston LE, Smith EJ, Little DG. Low-intensity ultrasound stimulation in distraction osteogenesis in rabbits. *Clin Orthop.* 2003;417:303-12.
15. Magyar G, Ahi TL, Vibe P, Toksvig-Larsen S, Lindstrand A. Open-wedge osteotomy by hemicallotasis or the closed-wedge technique for osteoarthritis of the knee. A randomised study of 50 operations. *J Bone Joint Surg Br.* 1999;81:444-8.
16. Magyar G, Toksvig-Larsen S, Lindstrand A. Hemicallotasis open-wedge osteotomy for osteoarthritis of the knee. Complications in 308 operations. *J Bone Joint Surg Br.* 1999;81:449-51.
17. Kellgren JH, Lawrence JS. Radiological assessment of osteoarthrosis. *Ann Rheum Dis.* 1957;16:494-502.
18. Sato W, Matsushita T, Nakamura K. Acceleration of increase in bone mineral content by low-intensity ultrasound energy in leg lengthening. *J Ultrasound Med.* 1999;18:699-702.
19. Maffulli N, Cheng JC, Sher A, Lam TP. Dual-energy X-ray absorptiometry predicts bone formation in lower limb callotasis lengthening. *Ann R Coll Surg Engl.* 1997;79:250-6.
20. Sakurakichi K, Tsuchiya H, Uehara K, Yamashiro T, Tomita K, Azuma Y. Effects of timing of low-intensity pulsed ultrasound on distraction osteogenesis. *J Orthop Res.* 2004;22:395-403.
21. Parvizi J, Parpura V, Greenleaf JF, Bolander ME. Calcium signaling is required for ultrasound-stimulated aggrecan synthesis by rat chondrocytes. *J Orthop Res.* 2002;20:51-7.
22. Parvizi J, Wu CC, Lewallen DG, Greenleaf JF, Bolander ME. Low-intensity ultrasound stimulates proteoglycan synthesis in rat chondrocytes by increasing aggrecan gene expression. *J Orthop Res.* 1999;17:488-94.
23. Naruse K, Miyauchi A, Itoman M, Mikuni-Takagaki Y. Distinct anabolic response of osteoblast to low-intensity pulsed ultrasound. *J Bone Miner Res.* 2003;18:360-9.
24. Li JK, Chang WH, Lin JC, Ruaan RC, Liu HC, Sun JS. Cytokine release from osteoblasts in response to ultrasound stimulation. *Biomaterials.* 2003;24:2379-85.
25. Ito M, Azuma Y, Ohta T, Komoriya K. Effects of ultrasound and 1,25-dihydroxyvitamin D3 on growth factor secretion in co-cultures of osteoblasts and endothelial cells. *Ultrasound Med Biol.* 2000;26:161-6.
26. Kokubo T, Matsui N, Fujioke H, Tsunoda M, Mizuno K. Low intensity pulsed ultrasound exposure increases prostaglandin E2 production via the induction of cyclooxygenase-2 mRNA in mouse osteoblasts. *Biochem Biophys Res Commun.* 1999;256:284-7.
27. Rawool NM, Goldberg BB, Forsberg F, Winder AA, Huma E. Power Doppler assessment of vascular changes during fracture treatment with low-intensity ultrasound. *J Ultrasound Med.* 2003;22:145-53.
28. Yasui N, Sato M, Ochi T, Kimura T, Kawahata H, Kitamura Y, Nomura S. Three modes of ossification during distraction osteogenesis in the rat. *J Bone Joint Surg Br.* 1997;79:824-30.



## Enhanced Generation of Endothelial Cells From CD34+ Cells of the Bone Marrow in Rheumatoid Arthritis

### Possible Role in Synovial Neovascularization

Shunsei Hirohata,<sup>1</sup> Tamiko Yanagida,<sup>1</sup> Akihide Nampei,<sup>2</sup> Yasuo Kunugiza,<sup>2</sup> Hideo Hashimoto,<sup>2</sup> Tetsuya Tomita,<sup>2</sup> Hideki Yoshikawa,<sup>2</sup> and Takahiro Ochi<sup>3</sup>

**Objective.** To examine the capacity of bone marrow CD34+ cells to generate endothelial cells, in order to assess the role of bone marrow in neovascularization in the synovium of rheumatoid arthritis (RA).

**Methods.** CD34+ cells purified from the bone marrow of 13 patients with active RA and 9 control subjects (7 osteoarthritis [OA] patients and 2 healthy individuals) were cultured in the presence of stem cell factor (10 ng/ml) and granulocyte-macrophage colony-stimulating factor (1 ng/ml). After 18 days of incubation, the generation of endothelial cells was assessed by flow cytometry. The generation of endothelial cells was compared with the degree of vascularization in the synovial tissues and with the microvessel densities in the synovium, as determined by microscopy. The expression of vascular endothelial growth factor receptor 2/kinase insert domain receptor (KDR) messenger RNA (mRNA) in CD34+ cells was examined by quantitative reverse transcription-polymerase chain reaction.

**Results.** The generation of CD14+ cells from bone marrow-derived CD34+ cells from RA patients was comparable to that from control subjects. However, the

generation of von Willebrand factor (vWF)-positive cells and CD31+/vWF+ cells from RA bone marrow-derived CD34+ cells was significantly higher than that from control subjects ( $P = 0.004$  and  $P = 0.030$ , respectively). The generation of vWF+ cells from bone marrow CD34+ cells correlated significantly with the microvessel densities in the synovial tissues ( $r = 0.569$ ,  $P = 0.021$ ). Finally, RA bone marrow CD34+ cells expressed KDR mRNA at higher levels than OA bone marrow CD34+ cells.

**Conclusion.** These results indicate that RA bone marrow CD34+ cells have enhanced capacities to differentiate into endothelial cells in relation to synovial vascularization. The data therefore suggest that bone marrow CD34+ cells might contribute to synovial neovascularization by supplying endothelial precursor cells and, thus, play an important role in the pathogenesis of RA.

Rheumatoid arthritis (RA) is a chronic inflammatory disease characterized by hyperplasia of synovial lining cells (1). Synovial lining cells consist of type A (macrophage-like) synoviocytes and type B (fibroblast-like) synoviocytes. Recent studies have suggested that type A synoviocytes are derived from monocyte precursors in the bone marrow (2). Accordingly, it has been shown that the spontaneous generation of CD14+ cells from bone marrow-derived CD14- progenitor cells is accelerated in RA, resulting in the facilitated entry of such CD14+ cells into the synovium (3). On the other hand, type B synoviocytes have a morphologic appearance of fibroblasts as well as the capacity to produce and secrete a variety of factors, including proteoglycans, cytokines, arachidonic acid metabolites, and matrix met-

Supported by a grant from the Ministry of Health, Labor, and Welfare of Japan.

<sup>1</sup>Shunsei Hirohata, MD, Tamiko Yanagida, PhD: Teikyo University School of Medicine, Tokyo, Japan; <sup>2</sup>Akihide Nampei, MD, PhD, Yasuo Kunugiza, MD, PhD, Hideo Hashimoto, MD, PhD, Tetsuya Tomita, MD, PhD, Hideki Yoshikawa, MD: Osaka University Medical School, Osaka, Japan; <sup>3</sup>Takahiro Ochi, MD: Sagami National Hospital, Kanagawa, Japan.

Address correspondence and reprint requests to Shunsei Hirohata, MD, Department of Internal Medicine, Teikyo University School of Medicine, 2-11-1 Kaga, Itabashi-ku, Tokyo 173-8605, Japan. E-mail: shunsei@med.teikyo-u.ac.jp.

Submitted for publication February 19, 2004; accepted in revised form September 2, 2004.

alloproteinases (MMPs), that lead to the destruction of joints (4). Whereas type B synoviocytes are thought to arise from the sublining tissue or other support structures of the joint (4), recent studies have suggested that they are also derived from bone marrow progenitor cells (5). Increasing attention has therefore been given to the role of the bone marrow in the pathogenesis of RA (6).

In the RA joint, the massive proliferating synovium forms an invading tissue called pannus, which results in the destruction of cartilage and bone. A number of studies have shown that persistent neovascularization is a crucial support to the continuous proliferation of the synovium, through delivery of nutrients and recruitment of inflammatory cells into the synovium (7,8). It was a long-held belief that vessels in the embryo developed from endothelial progenitors (vasculogenesis), whereas spouting of vessels in the adult resulted only from division of differentiated endothelial cells (angiogenesis) (9). Thus, the neovascularization in RA synovium has been attributed to angiogenesis, a process characterized by spouting of new capillaries from preexisting blood vessels (10).

Asahara et al (11), however, isolated endothelial progenitor cells from adult human peripheral blood using magnetic bead selection of CD34+ hematopoietic cells, and thus demonstrated that human peripheral blood CD34+ cells differentiated *in vitro* into endothelial cells, which expressed endothelial markers, including CD31. In addition, those investigators found that human CD34+ cells were incorporated into neovascularized hind limb ischemic sites in animal models (11). Since the time these observations were reported, it has also been found that endothelial progenitor cells capable of contributing to capillary formation can be derived from the bone marrow, possibly playing a role in the *de novo* formation of capillaries without preexisting blood vessels (12–14). Thus, the accumulating evidence has suggested that bone marrow-derived endothelial cells might be involved in several disorders characterized by excessive angiogenesis, such as myocardial infarction (15). However, the role of bone marrow in RA synovial neovascularization has not been explored.

It has been demonstrated that early endothelial progenitor cells in bone marrow express CD34, CD133, and vascular endothelial growth factor receptor 2 (VEGFR-2)/kinase insert domain receptor (KDR) (15). In general, early endothelial progenitor cells in the bone marrow are positive for CD34/CD133/VEGFR-2, whereas circulating endothelial progenitor cells are positive for CD34/VEGFR-2/CD31, negative for CD133,

and are beginning to express von Willebrand factor (vWF) (15). Thus, it appears that vWF is expressed on fully matured endothelial cells.

The current studies were undertaken to explore whether CD34+ cells derived from the bone marrow of RA patients might have an enhanced capacity to generate endothelial cells so that we could assess the role of the bone marrow in the neovascularization of RA synovium. The results clearly indicate that bone marrow-derived CD34+ cells from RA patients differentiate into vWF+ endothelial cells upon stimulation with stem cell factor (SCF) and granulocyte-macrophage colony-stimulating factor (GM-CSF) much more effectively than do those from control subjects. The data therefore suggest that bone marrow CD34+ cells might play a role in the synovial hyperplasia in RA through mobilization of endothelial progenitor cells into the synovium, where angiogenesis is activated.

## MATERIALS AND METHODS

**Patients and samples.** Bone marrow samples from 13 RA patients (1 man and 12 women; mean age 58.2 years [age range 45–72 years]) were obtained during joint operation through aspiration from the iliac crest. All RA patients met the American College of Rheumatology (formerly, the American Rheumatism Association) 1987 revised criteria (16). As controls, bone marrow samples were similarly obtained from 7 patients with osteoarthritis (OA) (7 women; mean age 70.6 years [age range 67–74]). All study patients gave their informed consent for study. In addition, bone marrow-derived CD34+ cells from 2 healthy individuals (2 men; ages 27 years and 24 years) were purchased from BioWhittaker (Walkersville, MD). Synovial tissues were also obtained from 10 of the RA patients and 6 of the OA patients during the same joint operation.

A second group of bone marrow samples was obtained from an additional 10 RA patients (3 men and 7 women; mean age 62.6 years) and an additional 4 OA patients (2 men and 2 women; mean age 72.6 years). These bone marrow samples were used in analyses of the expression of KDR messenger RNA (mRNA). These patients also gave their informed consent for study. In addition, samples from 7 of the RA patients and 6 of the OA patients from the first group described above were included in the study of KDR mRNA expression.

**Culture medium and reagents.** RPMI 1640 medium (Life Technologies, Grand Island, NY) supplemented with penicillin G (100 units/ml), streptomycin (100 µg/ml), L-glutamine (0.3 mg/ml), and 10% fetal bovine serum (Life Technologies) was used for all cultures. Recombinant human GM-CSF and SCF were purchased from PeproTech (London, UK).

**Preparation and culture of bone marrow-derived CD34+ cells.** Mononuclear cells were isolated by centrifugation of heparinized bone marrow aspirates over sodium



**Figure 1.** Histologic features (A) and immunohistochemistry of CD31 cells (B) in the synovium of patients with osteoarthritis (OA) and rheumatoid arthritis (RA). Four representative samples of synovium from OA (a and b) and RA (c and d) patients are presented, showing trace (a), mild (b), moderate (c), and strong (d) neovascularization. H&E = hematoxylin and eosin. (Original magnification  $\times 25$ .)

diatrizoate-Ficoll gradients (Histopaque; Sigma, St. Louis, MO). CD34+ cells were purified from the mononuclear cells through positive selection using magnetic beads (DynaL CD34 progenitor cell selection system; Dynal, Oslo, Norway). CD34+ cells thus prepared were  $\sim 95\%$  CD34+ cells and  $< 0.5\%$  CD19+ B cells, as previously described (5).

CD34+ cells were incubated in a 24-well microtiter plate with flat-bottomed wells (no. 3524; Costar, Cambridge, MA) at a density of  $1.0 \times 10^5$ /well in the presence of SCF (10 ng/ml) and GM-CSF (1 ng/ml). After 18 days of incubation, the cells were stained with various antibodies and analyzed by flow cytometry.

**Immunofluorescence staining and analysis.** Cultured CD34+ cells were stained with saturating concentrations of antibodies, including fluorescein isothiocyanate (FITC)-conjugated anti-HLA-DR monoclonal antibody (mAb) (mouse IgG2b; Immunotech, Marseilles, France), FITC-conjugated sheep anti-vWF IgG (Cosmo Bio, Tokyo, Japan), phycoerythrin (PE)-conjugated anti-CD14 mAb (mouse IgG2a; Immunotech), PE-conjugated anti-CD31 mAb (mouse IgG1; Immunotech), PE-conjugated murine IgG1 and IgG2a control mAb or FITC-conjugated murine IgG2b control mAb, which were raised against *Aspergillus niger* glucose oxidase, an enzyme that is neither present nor inducible in mammalian tissues (Dako, Glostrup, Denmark), or FITC-conjugated control sheep IgG purified from normal sheep serum (Rockland, Gilbertsville, PA).

Briefly, the cells were washed with 2% normal human serum in phosphate buffered saline (PBS), pH 7.2, and 0.1% sodium azide (staining buffer), and the cells were stained with saturating concentrations of a variety of antibodies at 4°C for 30 minutes. The cells were then washed 3 times with staining buffer and fixed with 1% paraformaldehyde in PBS for at least 5 minutes at room temperature. Cells were analyzed using an

Epics XL flow cytometer (Coulter, Hialeah, FL) equipped with an argon-ion laser at 488 nm. A combination of low-angle and 90° light scatter measurements (forward scatter versus side scatter) was used to identify bone marrow cells. The percentages of cells that stained positive for each mAb were determined by integration of cells above a specified fluorescence channel, which was calculated in relation to an isotype-matched control mAb.

**Synovial histopathology and determination of microvessel densities.** Synovial tissues were fixed in formalin, embedded in paraffin, and stained with hematoxylin and eosin. To visualize endothelial cells in the synovium, the paraffin-embedded sections were also stained with murine anti-CD31 mAb (clone JC/70A; Dako) and then developed using a Dako Envision kit, which includes horseradish peroxidase and diaminobenzidine. The degree of neovascularization was analyzed under light microscopy and scored as 0 (trace), 1 (mild), 2 (moderate), or 3 (strong) (Figures 1A and B). Grades were assigned by 2 independent observers (SH and TY) who had no knowledge of the diagnosis of the patients from whom the tissues had been obtained. When grades differed (2 of 16 cases), the synovium was reexamined, and a consensus was reached.

Sections were photographed with an Olympus DP11 digital camera (Olympus, Tokyo, Japan), and the CD31+ microvessel densities were determined by counting the vascular structures with a clearly defined lumen or linear shape as seen on the photographs. The final microvessel density was calculated as the mean score of the 3 1-mm<sup>2</sup> fields with the highest individual scores (17).

**Measurement of cytokines in the culture supernatants.** Concentrations of tumor necrosis factor  $\alpha$  (TNF $\alpha$ ) and vascular endothelial growth factor (VEGF) in the culture supernatants were measured by enzyme-linked immunosorbent assay

(ELISA) using a human TNF $\alpha$  ELISA kit (PeproTech) and a human VEGF immunoassay kit (BioSource International, Camarillo, CA).

**RNA isolation and real-time quantitative polymerase chain reaction.** Total RNA was isolated from purified bone marrow CD34+ cells using TRIzol reagent (Life Technologies) according to the manufacturer's instructions. Complementary DNA (cDNA) samples were prepared from 1  $\mu$ g of total RNA using the SuperScript reverse transcriptase preamplification system (Life Technologies) with oligo(dT) primers and were subjected to PCR. Real-time quantitative PCR was performed using the LightCycler rapid thermal cycler system (Roche Diagnostics, Lewes, UK) with primer sets for VEGFR-2/KDR or  $\beta$ -actin (Nihon Gene Research Laboratories, Sendai, Japan) and LightCycler FastStart DNA Master SYBR Green I (Roche Diagnostics).

The primer sequences were as follows: for KDR, 5'-CAGACGGACAGTGGTATGGT-3' (forward) and 5'-GCCTTCAGATGCCACAGACT-3' (reverse); and for  $\beta$ -actin, 5'-GCAAAGACCTGTACGCCAAC-3' (forward) and 5'-CTAGAAGCATTTCGGGTGGA-3' (reverse). The PCR reaction conditions were as follows: denaturing at 95°C for 10 minutes for 1 cycle, followed by 40 cycles of denaturing at 95°C for 10

seconds, annealing at 62°C for 10 seconds, and extension at 72°C for 5 seconds (KDR) or 10 seconds ( $\beta$ -actin). Quantitative analysis was performed using LightCycler software version 3.5. All results for KDR were calibrated to the copy number of  $\beta$ -actin from each cDNA sample.

RESULTS

**Synovial histopathologic features in RA.** A number of studies have confirmed that the microscopic appearance of RA synovial tissue is variable (18). Consistent with those studies, Figures 1A and B show representative patterns of neovascularization seen in RA synovium in this study. It appears that the overall degree of neovascularization is correlated with the degree of exudation, cellular infiltration, and granulation tissue development, which are characteristic features of RA synovium (18). Thus, synovium with marked granulation and cellular infiltration showed the maximal degree of neovascularization (Figures 1A and B part

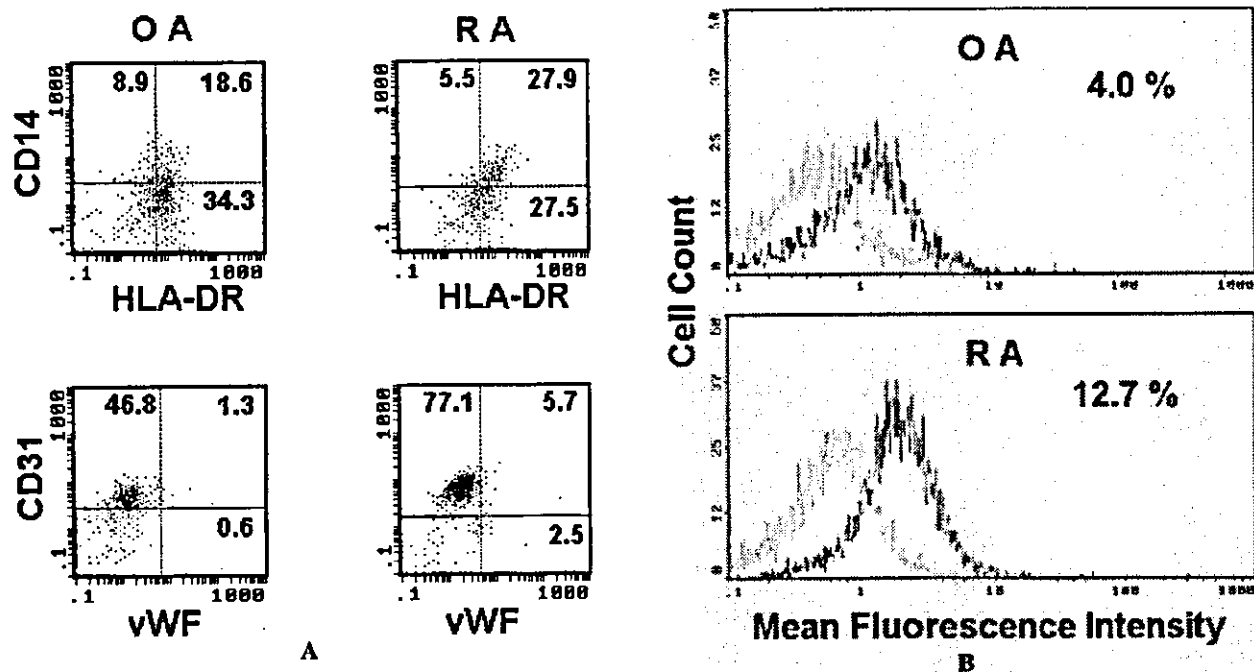


**Figure 2.** Representative 2-color and single-color flow cytometric analyses of the phenotypes of CD34+ cells stimulated with stem cell factor (SCF) and granulocyte-macrophage colony-stimulating factor (GM-CSF). CD34+ cells from the bone marrow of a rheumatoid arthritis (RA) and an osteoarthritis (OA) patient were stimulated for 18 days with SCF and GM-CSF, stained with phycoerythrin (PE)-conjugated anti-CD14 and fluorescein isothiocyanate (FITC)-conjugated anti-HLA-DR or with PE-conjugated anti-CD31 and FITC-conjugated von Willebrand factor (vWF), and analyzed by flow cytometry. **A**, The quadrant boundaries were determined by analysis of isotype-matched control cells. Values shown are percentages of cells. **B**, Single-color analysis of the expression of vWF (left histogram). Right histogram shows control staining. Percentages shown are for vWF+ cells. Figure 2B can be viewed in color in the online issue, which is available at <http://www.arthritisrheum.org>.

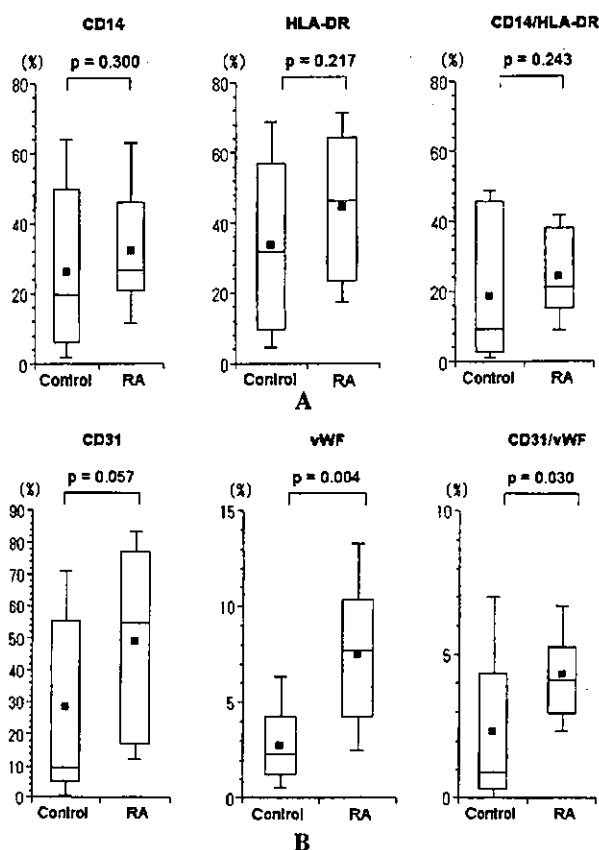


**Figure 3.** Phenotypic features of bone marrow-derived CD34+ cells stimulated with SCF and GM-CSF. Bone marrow CD34+ cells from 13 RA patients and 9 control subjects were stimulated for 18 days with SCF and GM-CSF, stained with A, PE-conjugated anti-CD14 and FITC-conjugated anti-HLA-DR or B, PE-conjugated anti-CD31 and FITC-conjugated anti-vWF, and analyzed by flow cytometry. Data are shown as box plots. Horizontal lines constituting the top, middle, and bottom of the boxes show the 75th, 50th, and 25th percentiles, respectively. Lines outside the boxes show the 90th and 10th percentiles. Solid squares inside the boxes show the mean. *P* values were determined by Mann-Whitney U test. See Figure 2 for definitions.

d), whereas the synovium with trace amounts of exudation and cellular infiltration lacked neovascularization. The results therefore suggest that neovascularization might play a role in development of inflamed synovium in RA.

**Generation of vWF+ cells from bone marrow-derived CD34+ cells.** After stimulation of bone marrow CD34+ cells ( $1.0 \times 10^5$ ) with SCF and GM-CSF for 18 days, the mean  $\pm$  SD number of recovered cells was  $3.85 \pm 2.97 \times 10^5$  for RA patients and  $3.79 \pm 3.18 \times$

$10^5$  for control subjects ( $P = 0.6401$  by Mann-Whitney U test). Figures 2A and B show, respectively, the representative dual-parameter 4-quadrant scattergrams and single-color histograms of the bone marrow CD34+ cells stimulated with SCF and GM-CSF for 18 days.

A similar percentage of cultured CD34+ cells from the RA patient and the OA control patient expressed CD14 and HLA-DR. Although in Figure 2A, bone marrow CD34+ cells from the RA patient generated higher percentages of CD14+/HLA-DR+ cells, there was no significant difference in the percentages of CD14+ cells and CD14+/HLA-DR+ cells generated by bone marrow CD34+ cells from the 9 control subjects and the 13 RA patients (Figure 3A). In contrast, bone marrow CD34+ cells from the RA patient gave rise to higher numbers of vWF+ cells and CD31+/vWF+ cells than did those from the OA control patient (Figures 2A

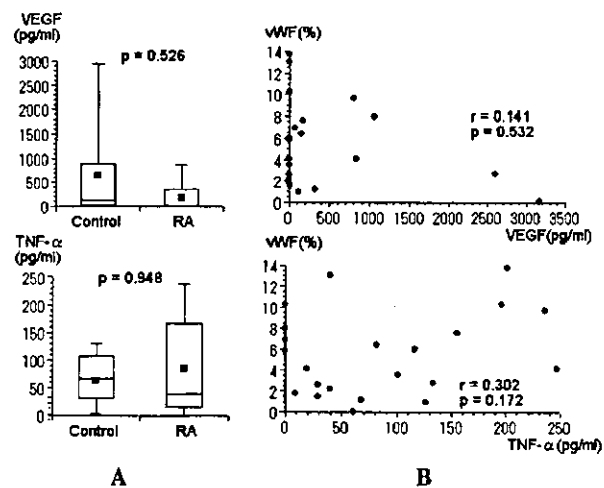


**Figure 4.** Production of vascular endothelial growth factor (VEGF) and tumor necrosis factor  $\alpha$  (TNF $\alpha$ ) by bone marrow-derived CD34+ cells and correlation with the generation of von Willebrand factor (vWF)-positive cells. Bone marrow CD34+ cells from 13 rheumatoid arthritis (RA) patients and 9 control subjects were stimulated for 18 days with stem cell factor and granulocyte-macrophage colony-stimulating factor. Cells were analyzed for vWF expression by flow cytometry; supernatants were assayed for VEGF and TNF $\alpha$  by enzyme-linked immunosorbent assay. A, Data are shown as box plots. Horizontal lines constituting the top, middle, and bottom of the boxes show the 75th, 50th, and 25th percentiles, respectively. Lines outside the boxes show the 90th and 10th percentiles. Solid squares inside the boxes show the mean. *P* values were determined by Mann-Whitney U test. B, Correlations between the generation of vWF+ cells and the production of each cytokine was evaluated by simple regression analysis.

and B). Accordingly, bone marrow CD34+ cells from the 13 RA patients generated significantly higher numbers of vWF+ cells as well as CD31+/vWF+ cells than did those from the 9 control subjects, although there was no significant difference in the number of CD31+ cells (Figure 3B). These results indicate that upon stimulation with SCF and GM-CSF, bone marrow CD34+ cells from RA patients have enhanced capacities to generate endothelial cells compared with control subjects, whereas the capacities of RA bone marrow CD34+ cells to give rise to CD14+ monocyte-lineage cells were comparable to those of the control subjects.

**Relationship between the generation of vWF+ cells and the production of VEGF and TNF $\alpha$ .** It was possible that the enhanced generation of vWF+ cells from RA bone marrow-derived CD34+ cells might be a result of the increased production of angiogenic cytokines. In fact, it has been reported that VEGF (19,20) and TNF $\alpha$  (21–24) play a major role in regulating neovascularization in RA. Our next experiments therefore examined the capacity of bone marrow CD34+ cells stimulated with SCF plus GM-CSF to produce VEGF and TNF $\alpha$ . As can be seen in Figure 4, there were no significant differences in the production of VEGF and TNF $\alpha$  by RA bone marrow CD34+ cells and control bone marrow CD34+ cells. In addition, the generation of vWF+ cells was not significantly correlated with the production of VEGF or TNF $\alpha$ . The results therefore suggest that the enhanced generation of vWF+ cells from RA bone marrow CD34+ cells might not be due to the increased production of angiogenic cytokines but, more likely, it may be due to the intrinsic abnormalities of the bone marrow CD34+ cells.

**Relationship between the capacity of bone marrow-derived CD34+ cells to generate endothelial cells and the vascularization of the synovium.** To further confirm the role of the bone marrow in synovial neovascularization, we next examined the relationship between the capacity of bone marrow CD34+ cells to generate vWF+ cells and the degree of vascularization in the synovium in synovium samples obtained from 10 of the RA patients and 6 of the OA patients on the same day as the bone marrow samples. The degree of vascularization in the synovium was analyzed under light microscopy and scored as described in Materials and Methods. The degree of synovial vascularization in the RA patients was significantly elevated compared with that in the OA patients. In addition, the capacity of bone marrow CD34+ cells to generate vWF+ cells was significantly

correlated with the degree of vascularization in the synovium in these 16 patients (data not shown).

To evaluate the synovial vascularization in a more objective manner, we calculated the CD31+ microvessel densities in the synovium. As shown in Figure 5, the synovial microvessel densities were significantly higher in RA patients than in OA patients. Moreover, the microvessel densities were also significantly correlated with the generation of vWF+ cells from bone marrow-derived CD34+ cells in the 16 patients with OA or RA. The results therefore suggest that vasculogenesis occurring through mobilization of endothelial progenitor cells from the bone marrow might be involved, at least in part, in the synovial neovascularization, and may thus play a significant role in the pathogenesis of RA.

**Expression of mRNA for VEGFR-2/KDR in bone marrow-derived CD34+ cells.** Recent studies have revealed that the vascular activation by VEGF/KDR was significantly higher in RA than in OA, although activation of the hypoxia inducing factor  $\alpha$  (HIF $\alpha$ ) pathway was comparable in RA and OA (25). It was therefore possible that there might be differences in the activation

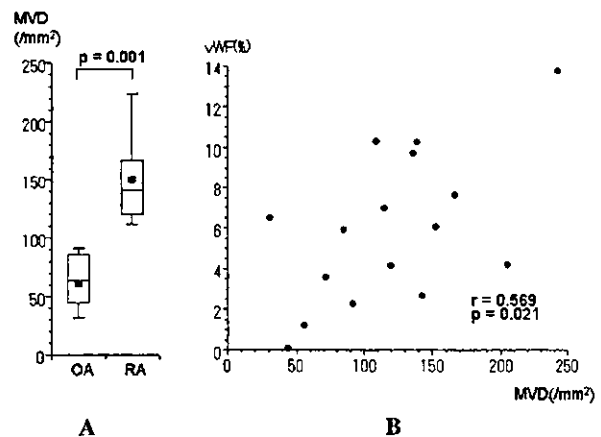


**Figure 5.** Correlation between synovial microvessel densities (MVD) and the generation of von Willebrand factor (vWF)-positive cells from bone marrow-derived CD34+ cells. Synovial microvessel densities were compared between 10 rheumatoid arthritis (RA) patients and 6 osteoarthritis (OA) patients. **A**, Data are shown as box plots. Horizontal lines constituting the top, middle, and bottom of the boxes show the 75th, 50th, and 25th percentiles, respectively. Lines outside the boxes show the 90th and 10th percentiles. Solid squares inside the boxes show the mean. *P* values were determined by Mann-Whitney U test. **B**, Correlations between the microvessel densities and the generation of vWF+ cells from bone marrow CD34+ cells in the 16 patients was determined by simple regression analysis.

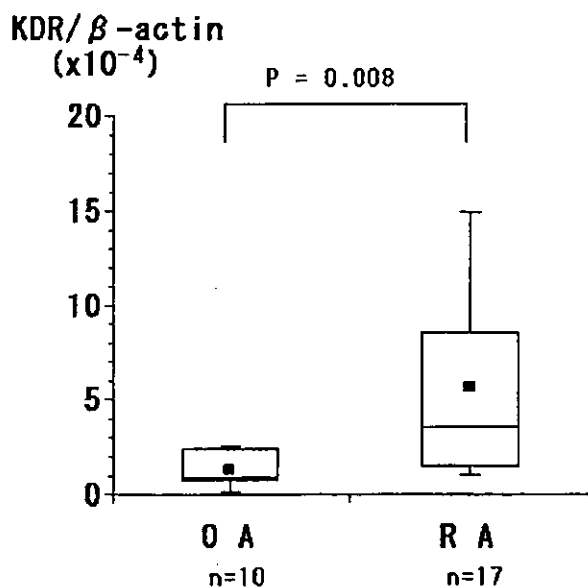


**Figure 6.** The expression of vascular endothelial growth factor receptor 2 (VEGFR-2)/kinase insert domain receptor (KDR) mRNA in bone marrow-derived CD34+ cells. RNA was extracted from bone marrow CD34+ cells obtained from rheumatoid arthritis (RA) and osteoarthritis (OA) patients and subjected to quantitative reverse transcription-polymerase chain reaction for VEGFR-2/KDR. The copy numbers for VEGFR-2/KDR mRNA were calibrated to those for  $\beta$ -actin. Data are shown as box plots. Horizontal lines constituting the top, middle, and bottom of the boxes show the 75th, 50th, and 25th percentiles, respectively. Lines outside the boxes show the 90th and 10th percentiles. Solid squares inside the boxes show the mean. *P* values were determined by Mann-Whitney U test.

of the VEGF/KDR pathway in bone marrow CD34+ cells. To explore this possibility, our final experiments examined the expression of KDR mRNA in bone marrow CD34+ cells as measured by quantitative reverse transcription-PCR. As can be seen in Figure 6, the expression of VEGFR-2/KDR mRNA in bone marrow CD34+ cells from 17 patients with RA was significantly higher than that in bone marrow CD34+ cells from 10 patients with OA. The results therefore suggest that up-regulation of KDR mRNA in bone marrow CD34+ cells in RA might result in their enhanced capacity to generate endothelial cells.

## DISCUSSION

A number of studies have indicated that neovascularization is crucial to the synovial hyperplasia of RA (7,8). Postnatal neovascularization has been attributed

to so-called angiogenesis, a process characterized by the sprouting of new capillaries from preexisting blood vessels (10). Thus, it has been shown that the expression of angiogenic factors, such as VEGF and basic fibroblast growth factor in synovial lining cells and stromal cells, is increased in RA synovium and plays a pivotal role in the angiogenesis (19,20,23). It is noteworthy that recent studies have demonstrated that endothelial progenitor cells of bone marrow origin play a significant role in the de novo formation of capillaries without preexisting blood vessels, so-called vasculogenesis (11-14). Moreover, bone marrow-derived endothelial precursor cells have been shown to home to neovascularized hind limb ischemic sites in animal models (11). Results of the current studies have shown that the generation of vWF+ endothelial cells from bone marrow CD34+ cells is up-regulated in RA. The data therefore suggest that mobilization of endothelial cells from bone marrow might also be enhanced and be involved in neovascularization of the RA synovium. It is thus likely that bone marrow-derived endothelial precursor cells might be homing to the synovium, where angiogenesis is enhanced (7,8).

It has been shown that bone marrow-derived endothelial progenitor cells make a significant contribution to angiogenic growth factor-induced neovascularization that may account for up to 26% of all endothelial cells (26,27). It is therefore likely that the enhanced capacity of bone marrow CD34+ cells to generate vWF+ cells might also play a critical role in the synovial neovascularization in RA. In fact, we found that the degree of synovial vascularization as well as the microvessel densities in RA synovium were much higher than those in OA synovium, findings that are consistent with those of a previous study (28). More important, the generation of vWF+ cells from bone marrow-derived CD34+ cells was significantly correlated with the degree of synovial vascularization as well as with the microvessel densities in arthritis patients. The data therefore raise the possibility that the mobilization of endothelial progenitor cells from bone marrow might also contribute to the enhanced synovial neovascularization in RA, although a direct role for these bone marrow-derived cells in synovial neovascularization remains to be elucidated. Further studies to explore in detail the capacity of endothelial progenitor cells generated from bone marrow CD34+ cells to undergo angiogenesis would be important.

Previous studies have shown that hematopoietic cytokines, such as SCF and GM-CSF, have potent

effects on endothelial cells and facilitate angiogenesis (29). In the current studies, we demonstrated that SCF and GM-CSF also induce the generation of endothelial cells from bone marrow CD34+ cells and, thus, participate in vasculogenesis. The mechanism of the enhanced generation of endothelial cells from RA bone marrow CD34+ cells stimulated with SCF and GM-CSF is still unclear. It is possible that the production of VEGF, presumably by CD14+ cells induced from CD34+ cells, might be enhanced in cultures of RA bone marrow-derived CD34+ cells. However, there were no significant differences in the production of VEGF between RA patients and control subjects. Moreover, the generation of vWF+ cells was not significantly correlated with the production of VEGF. It is therefore unlikely that the enhanced generation of vWF+ cells from RA bone marrow CD34+ cells might result from the up-regulation of VEGF production.

TNF $\alpha$  plays a crucial role in regulating not only inflammation, but also neovascularization in RA synovium (21–24). Anti-TNF $\alpha$  treatment in RA patients has been found to inhibit vascularity in the synovium (30,31). The results of the current studies revealed that significant amounts of TNF $\alpha$  were produced in cultures of bone marrow CD34+ cells. However, there were no significant differences in the production of TNF $\alpha$  by bone marrow CD34+ cells from RA patients and control subjects, nor was the generation of vWF+ cells significantly correlated with the production of TNF $\alpha$ . Therefore, the enhanced generation of vWF+ cells might not be accounted for by the increased production of TNF $\alpha$ , although it is still possible that up-regulation of the production of angiogenic factors other than VEGF and TNF $\alpha$  might be involved in the enhanced generation of vWF+ cells from RA bone marrow CD34+ cells. Alternatively, it is also possible that the reactivity of RA bone marrow CD34+ cells to various cytokines might be different from that of control bone marrow CD34+ cells. In this regard, previous studies have shown that RA bone marrow CD34+ cells have abnormal capacities to respond to TNF $\alpha$  and differentiate into fibroblast-like cells producing MMP-1 (5).

Neovascularization of the synovium is not unique to RA. It has also been observed in OA synovium and has been shown to play an important role in the development of new cartilage and mineralization (25,32,33). Of note, recent studies have revealed that levels of expression of the angiogenic factors VEGF and platelet-derived endothelial cell growth factor are increased in RA as well as in OA, relative to normal subjects,

whereas the presence of an activated synovial vasculature was high only in RA (25). Moreover, the vascular activation by VEGF/KDR was significantly lower in OA than in RA patients, although the activation of the HIF $\alpha$  pathway was comparable in OA and RA patients (25). These observations suggest the presence of intrinsic abnormalities in synovial endothelial cells in RA patients. Of note, in the present study, RA bone marrow CD34+ cells displayed a higher capacity to generate vWF+ endothelial cells than did OA bone marrow CD34+ cells. Moreover, the expression of VEGFR-2/KDR mRNA in RA bone marrow CD34+ cells was significantly higher than that in OA bone marrow CD34+ cells. It is therefore likely that the differences in VEGF/KDR vascular activation at the level of bone marrow CD34+ cells between RA and OA patients might result in differences in their capacity to generate vWF+ cells, since signaling through the KDR plays a crucial role in the generation of endothelial cells (17,19). Further studies to delineate the precise sequelae of the up-regulation of KDR mRNA expression would be helpful for a complete understanding not only of the differences in synovial neovascularization in RA and OA, but also of the pathogenesis of RA.

## REFERENCES

1. Firestein GS, Zvaifler NJ. How important are T cells in chronic rheumatoid synovitis? *Arthritis Rheum* 1990;33:768–73.
2. Burmester GR, Stuhlmüller B, Keyszer G, Kinne RW. Mononuclear phagocytes and rheumatoid synovitis: mastermind or workhorse in arthritis? *Arthritis Rheum* 1997;40:5–18.
3. Hirohata S, Yanagida T, Itoh K, Nakamura H, Yoshino S, Tomita T, et al. Accelerated generation of CD14+ monocyte-lineage cells from the bone marrow of rheumatoid arthritis patients. *Arthritis Rheum* 1996;39:836–43.
4. Firestein GS. Invasive fibroblast-like synoviocytes in rheumatoid arthritis: passive responders or transformed aggressors? *Arthritis Rheum* 1996;39:1781–90.
5. Hirohata S, Yanagida T, Nagai T, Sawada T, Nakamura H, Yoshino S, et al. Induction of fibroblast-like cells from CD34+ progenitor cells of the bone marrow in rheumatoid arthritis. *J Leukoc Biol* 2001;70:413–21.
6. Berthelot JM, Bataille R, Maugars Y, Prost A. Rheumatoid arthritis as a bone marrow disorder. *Semin Arthritis Rheum* 1996;26:505–14.
7. Koch AE. Angiogenesis: implications for rheumatoid arthritis. *Arthritis Rheum* 1998;41:951–62.
8. Firestein GS. Starving the synovium: angiogenesis and inflammation in rheumatoid arthritis. *J Clin Invest* 1999;103:3–4.
9. Carmeliet P. Angiogenesis in health and disease. *Nat Med* 2003;9:653–60.
10. Folkman J, Shing Y. Angiogenesis. *J Biol Chem* 1992;267:10931–4.
11. Asahara T, Murohara T, Sullivan A, Silver M, van der Zee R, Li T, et al. Isolation of putative progenitor endothelial cells for angiogenesis. *Science* 1997;275:964–7.



12. Gehling UM, Ergun S, Schumacher U, Wagener C, Pantel K, Otte M, et al. In vitro differentiation of endothelial cells from AC133-positive progenitor cells. *Blood* 2000;95:3106-12.
13. Bhattacharya V, McSweeney PA, Shi Q, Bruno B, Ishida A, Nash R, et al. Enhanced endothelialization and microvessel formation in polyester grafts seeded with CD34<sup>+</sup> bone marrow cells. *Blood* 2000;95:581-5.
14. Lin Y, Weisdorf DJ, Solovey A, Hebbel RP. Origins of circulating endothelial cells and endothelial outgrowth from blood. *J Clin Invest* 2000;105:71-7.
15. Hristov M, Ertl W, Weber PC. Endothelial progenitor cells: mobilization, differentiation, and homing. *Arterioscler Thromb Vasc Biol* 2003;23:1185-9.
16. Arnett FC, Edworthy SM, Bloch DA, McShane DJ, Fries JF, Cooper NS, et al. The American Rheumatism Association 1987 revised criteria for the classification of rheumatoid arthritis. *Arthritis Rheum* 1988;31:315-24.
17. Giatromanolaki A, Sivridis E, Athanassou N, Zois E, Thorpe PE, Brekken RA, et al. The angiogenic pathway "vascular endothelial growth factor/flk-1 (KDR)-receptor" in rheumatoid arthritis and osteoarthritis. *J Pathol* 2001;194:101-8.
18. Hough AJ Jr. Pathology of rheumatoid arthritis and allied disorders. In: McCarty DJ, Koopman WJ, editors. *Arthritis and allied conditions: a textbook of rheumatology*. 12th ed. Philadelphia: Lea & Febiger; 1993. p. 737-61.
19. Koch AE, Harlow LA, Haines GK, Amento EP, Unemori EN, Wong WL, et al. Vascular endothelial growth factor: a cytokine modulating endothelial function in rheumatoid arthritis. *J Immunol* 1994;152:4149-56.
20. Fava RA, Olsen NJ, Spencer-Green G, Yeo KT, Yeo TK, Berse B, et al. Vascular permeability factor/endothelial growth factor (VPF/VEGF): accumulation and expression in human synovial fluids and rheumatoid synovial tissue. *J Exp Med* 1994;180:341-6.
21. Maini RN, Taylor PC, Paleolog E, Charles P, Ballara S, Brennan FM, et al. Anti-tumor necrosis factor specific antibody (infliximab) treatment provides insights into the pathophysiology of rheumatoid arthritis. *Ann Rheum Dis* 1999;58 Suppl 1:156-60.
22. McCourt M, Wang JH, Sookhai S, Redmond HP. Proinflammatory mediators stimulate neutrophil-directed angiogenesis. *Arch Surg* 1999;134:1325-31.
23. Fajardo LF, Kwan HH, Kowalski J, Prionas SD, Allison AC. Dual role of tumor necrosis factor- $\alpha$  in angiogenesis. *Am J Pathol* 1992;140:539-44.
24. Yoshida S, Ono M, Shono T, Izumi H, Ishibashi T, Suzuki H, et al. Involvement of interleukin-8, vascular endothelial growth factor, and basic fibroblast growth factor in tumor necrosis factor  $\alpha$ -dependent angiogenesis. *Mol Cell Biol* 1997;17:4015-23.
25. Giatromanolaki A, Sivridis E, Maltezos E, Athanassou N, Papanaglou D, Gatter KC, et al. Upregulated hypoxia inducible factor-1 $\alpha$  and -2 $\alpha$  pathway in rheumatoid arthritis and osteoarthritis. *Arthritis Res Ther* 2003;5:R193-201.
26. Takahashi T, Kalka C, Masuda H, Chen D, Silver M, Kearney M, et al. Ischemia- and cytokine-induced mobilization of bone marrow-derived endothelial progenitor cells for neovascularization. *Nat Med* 1999;5:434-8.
27. Murayama T, Tepper OM, Silver M, Ma H, Losordo DW, Isner JM, et al. Determination of bone marrow-derived endothelial progenitor cell significance in angiogenic growth factor-induced neovascularization in vivo. *Exp Hematol* 2002;30:967-72.
28. Neidhart M, Wehrli R, Bruhlmann P, Michel BA, Gay RE, Gay S. Synovial fluid CD146 (MUC18), a marker for synovial membrane angiogenesis in rheumatoid arthritis. *Arthritis Rheum* 1999;42:622-30.
29. Pelletier L, Regnard J, Fellmann D, Charbord P. An in vitro model for the study of human bone marrow angiogenesis: role of hematopoietic cytokines. *Lab Invest* 2000;80:501-11.
30. Criscione LG, St Clair EW. Tumor necrosis factor- $\alpha$  antagonists for the treatment of rheumatic diseases. *Curr Opin Rheumatol* 2002;14:204-11.
31. Feldmann M, Maini RN. Anti-TNF $\alpha$  therapy of rheumatoid arthritis: what have we learned? *Annu Rev Immunol* 2001;19:163-96.
32. Brown RA, Weiss JB, Tomlinson IW, Phillips P, Kumar S. Angiogenic factor from synovial fluid resembling that from tumours. *Lancet* 1980;1:682-5.
33. Haywood L, McWilliams DF, Pearson CI, Gill SE, Ganesan A, Wilson D, et al. Inflammation and angiogenesis in osteoarthritis. *Arthritis Rheum* 2003;48:2173-7.

# 新規全気孔連通型HA多孔体 NEOBONE<sup>®</sup>を用いた骨欠損 に対する治療

玉井宣行 名井 陽 荒木信人 秋田鐘彌 中瀬尚長 海渡貴司  
村瀬 剛 上田孝文 越智隆弘 吉川秀樹

Key words : hydroxyapatite ceramics, interconnected pore, bone graft

## はじめに

整形外科分野において骨腫瘍、外傷など種々の病変による骨欠損に対し、古くから骨盤や腓骨などからの自家骨移植が優れた方法として一般的に用いられてきたが、採骨に伴う手術侵襲、採骨部の創や疼痛、採骨部の術後骨折などの合併症があるうえに、絶対的な供給量に問題がある。近年自家骨に代わり、アルミナ、ジルコニア、バイオガラス、ハイドロキシアパタイト(HA)などさまざまな素材が人工骨として使用されてきている。そのなかでも、HAは哺乳類の骨、歯の無機質成分に類似しており、その生体親和性、骨伝導能をみても人工骨として非常に適していると考えられる。それらのことより、1980年代より整形外科、歯科口腔外科領域において骨補填剤としてHA多孔体が使用されている。

HA多孔体は当初その気孔内に新生骨が侵入し、母床骨と完全に同化することが期待されたが、HA多孔体が新生骨に完全に置換されるという報告はなく、むしろさまざまな臨床症例の解析から気孔内への新生骨侵入は数mm程度であることが明らかになってきた<sup>1)</sup>。このような新生骨が侵入しない気孔は強度面で非常に不利であり、HA多孔体移植後骨折を合併した症例の報告も見受けられる<sup>2)</sup>。これらは気孔と気孔を結ぶ連通構造に問題があり、深部への組織侵入、骨新生を阻害していたためと考えられる。

このような問題点を解決するためわれわれは物質・材料研究機構、東芝セラミックス株式会社、株式会社MMTとの共同開発で新しい製造法“起泡ゲル化技術”を取り入れ、新規HA多孔体を開発した。このHA多孔体は均一な気孔構造と適度な気孔間連通構造を特徴としている<sup>3),4)</sup>。本

Surgical treatment of bone defects with novel interconnected porous hydroxyapatite ceramics

0286-5394/04/¥400/論文/JCLS

N.Tamai, A.Myoui, T.Kaito, T.Murase, T.Ueda, T.Ochi, H.Yoshikawa : 大阪大学大学院医学系研究科器官制御外科学(整形外科); N.Araki : 大阪府立成人病センター整形外科; S.Akita : 星ヶ丘厚生年金病院整形外科; T.Nakase : 国立病院大阪医療センター整形外科

稿では、この新規HA多孔体(NEOBONE®)の特徴を述べ、臨床使用での良好な成績を紹介する。

## 新規HA多孔体(NEOBONE®)の開発

今回われわれが新規開発したNEOBONE®(図1 ③)は、気孔率75%、平均気孔径150ミクロン、初期強度12MPaであり、製法上の特徴は起泡ゲル化技術を取り入れたことである<sup>3)</sup>。起泡ゲル化技術とは、①HAスラリーに起泡剤を加えて一定の条件で攪拌することにより泡沫状のスラリーを作製し、②ポリエチレンイミンと水溶性の多官能基エポキシ化合物を組み合わせた架橋重合反応により、短時間で泡沫状のスラリーを

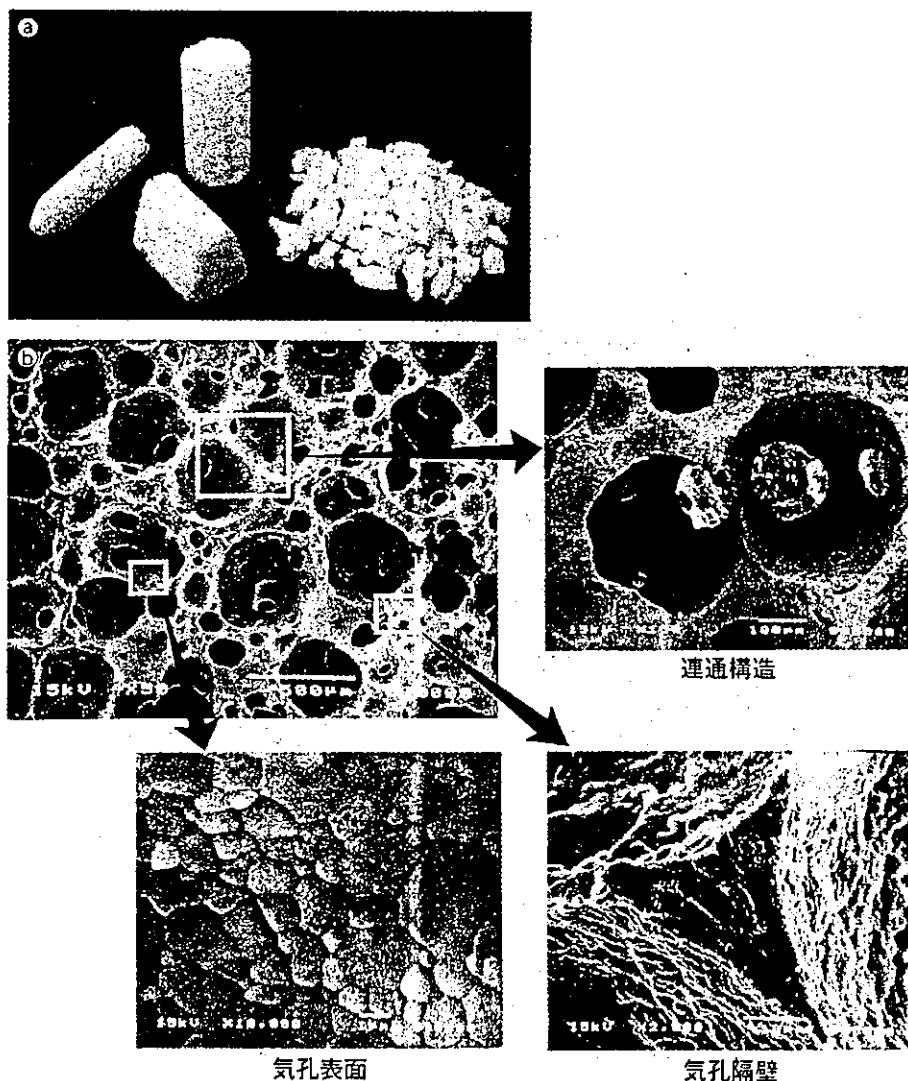
全域にわたって同時に固める手法である。

図1 ⑥にNEOBONE®の電子顕微鏡写真を示す。NEOBONE®の気孔は、ほぼ球形で比較的均一なサイズの気孔が規則正しく配列し、ほぼ全気孔が気孔間連通路で連絡した構造を有していた。気孔隔壁は10~20ミクロンを有し、その表面はHA粒子が密に秩序よく配列されていた。水銀圧入ポロシメトリーによる気孔の連通状態の検討では、連通路径分布は10~80ミクロン(平均40ミクロン)であり、NEOBONE®の気孔の約90%が細胞や組織が十分通過できる大きさの連通路でつながっていた。力学的強度は初期圧縮強度で10MPa以上で、臨床応用されている同等の気孔率を有するHA多孔体と比較して優れた数値を示した。この強度は電子顕微鏡所見か

図1 NEOBONE®とその構造

③：NEOBONE®のマクロ像。

⑥：NEOBONE®の電子顕微鏡写真。



らもわかるように気孔が均一でほぼ球形であり、骨格部分のHA粒子間の結合が強固であることによって得られたと考えられる。

直径6mmのNEOBONE®円柱ブロックを白色家兎大腿骨に移植し骨伝導能を検討した(図2 ㉔)。大腿骨に移植した多孔体内への組織の侵入を、三次元的に捉えるため、表層からの距離によりゾーン分けを行い、母床骨に接している円柱ブロックの最外側部1mmをゾーンS、母床骨より最も離れている最深部1mmをゾーンDとした(図2 ㉕)。移植後2週では、母床骨に接しているゾーンSで三日月状の無数の新生

骨が観察できた。ゾーンDでは、細胞浸潤がほとんどなく、血塊が大部分を占めていた。移植後3週では、ゾーンSでは新生骨髄も確認することができたが、ゾーンDでは一部に新生骨を認めるものの、血管新生を伴う肉芽組織が主であった。

移植後6週では、ゾーンSからゾーンDまでのすべての気孔に豊富な新生骨髄を伴う新生骨を確認することができ、非常に優れた骨伝導能を示した(図2 ㉖)。この骨新生に伴い圧縮強度は移植後9週で初期強度の3倍に達していた。

## 図2 NEOBONE®の骨伝導能

㉔：白色家兎大腿骨埋入実験(大腿骨顆部に直径6mmのドリルホールを開け、高さ15mmのNEOBONE®円柱を移植)。

㉕：ゾーン分け。

㉖：ゾーン別気孔内の骨形成(ヘマトキシリン・エオジン染色、×100)。

